

# Detection of multimode spatial correlation in PDC and application to the absolute calibration of a CCD camera

Giorgio Brida, Ivo Pietro Degiovanni, Marco Genovese, Maria Luisa Rastello, Ivano Ruo-Berchera\*

*Istituto Nazionale di Ricerca Metrologica, Strada delle Cacce 91, 10135 Torino, Italy*

[\\*i.ruoberchera@inrim.it](mailto:i.ruoberchera@inrim.it)

**Abstract:** We propose and demonstrate experimentally a new method based on the spatial entanglement for the absolute calibration of analog detector. The idea consists on measuring the sub-shot-noise intensity correlation between two branches of parametric down conversion, containing many pairwise correlated spatial modes. We calibrate a scientific CCD camera and a preliminary evaluation of the statistical uncertainty indicates the metrological interest of the method.

© 2010 Optical Society of America

**OCIS codes:** (270.4180) Multiphoton processes; (120.1880) Detection; (120.3940) Metrology.

---

## References and links

1. Quantum Imaging, Kolobov editor (Springer, New York, 2007), and ref.s therein.
2. Brambilla, E., Gatti, A., Bache, M., and Lugiato L. A. "Simultaneous near-field and far-field spatial quantum correlations in the high-gain regime of parametric down-conversion". *Phys. Rev. A* **69**, 023802 (2004).
3. J.-L. Blanchet *et al.*, "Measurement of Sub-Shot-Noise Correlations of Spatial Fluctuations in the Photon-Counting Regime", *Phys. Rev. Lett.* **101**, 233604 (2008).
4. O. Jedrkiewicz *et al.*, "Detection of Sub-Shot-Noise Spatial Correlation in High-Gain Parametric Down Conversion", *Phys. Rev. Lett.* **93**, 243601 (2004).
5. G. Brida *et al.*, "Measurement of Sub-Shot-Noise Spatial Correlations without Background Subtraction", *Phys. Rev. Lett.* **102**, 213602 (2009).
6. G. Brida, M. Genovese, I. Ruo Berchera, "Experimental realization of sub-shot-noise quantum imaging", *Nature Photonics* **4**, 227 - 230 (2010).
7. Bondani, M., Allevi, A., Zambra, G., Paris, M. and Andreoni, "A. Sub-shot-noise photon-number correlation in a mesoscopic twin beam of light", *Phys. Rev. A* **76**, 013833 (2007).
8. T. Ishakov, M. Chekhova, G. Leuchs, "Generation and Direct Detection of Broadband Mesoscopic Polarization-Squeezed Vacuum", *Phys. Rev. Lett.* **102**, 183602 (2009).
9. E. Brambilla, *et al.*, "High-sensitivity imaging with multi-mode twin beams", *Phys. Rev. A* **77**, 053807 (2008).
10. Boyer, V., Marino, A. M. and Lett, P. D. "Generation of spatially broadband twin beams for quantum imaging.", *Phys. Rev. Lett.* **100**, 143601 (2008).
11. M. Genovese, "Research on hidden variable theories: A review on recent progresses," *Phys. Rep.* **413/6**, 319-398 (2005) and references therein.
12. S. Polyakov and A. Migdall, "High accuracy verification of a correlated-photon- based method for determining photoncounting detection efficiency" *Opt. Exp.* **15** (4), 1390 (2007).
13. B.Y. Zel'dovich and D.N. Klyshko, "Statistics of field in parametric luminescence," *Sov. Phys. JETP Lett.* **9** 40-44 (1969).
14. D.C. Burnham and D.L. Weinberg, "Observation of Simultaneity in Parametric Production of Optical Photon Pairs," *Phys. Rev. Lett.* **25**, 84-87 (1970).
15. D.N. Klyshko, "Use of two-photon light for absolute calibration of photoelectric detectors," *Sov. J. Quant. Elect.* **10**, 1112-1116 (1980).

16. A. A. Malygin, A. N. Penin and A. V. Sergienko, "Absolute Calibration of the Sensitivity of Photodetectors Using a Two-Photon Field," *Sov. Phys. JETP Lett.* **33**, 477-480 (1981).
17. V. M. Ginzburg, N. G. Keratishvili, E. L. Korzhenevich, "Absolute meter of photodetector quantum efficiency based on the parametric down-conversion effect," G. V. Lunev, A. N. Penin, V. I. Sapritsky, *Opt. Eng.* **32**(11), 2911-2916 (1993).
18. A. Migdall, "Correlated-photon metrology without absolute standards," *Physics Today* January, 41-46 (1999).
19. M. Lindenthal and J. Kofler "Measuring of the absolute photodetection efficiency using photon number correlations" *App. Opt.* **45**(24),6059 (2006).
20. "AN APPLICATION OF TWO PHOTONS ENTANGLED STATES TO QUANTUM METROLOGY", M.Genovese, G. Brida e C. Novero. *Jour. Mod. Opt.* **47** (2000) 2099.
21. "TOWARD AN ACCURACY BUDGET IN QUANTUM EFFICIENCY MEASUREMENT WITH PARAMETRIC FLUORESCENCE", G. Brida, S. Castelletto, I. Degiovanni, M. Genovese, C. Novero e M.L. Rastello, *METROLOGIA* **37** 5 (2000) 629.
22. "SINGLE-PHOTON DETECTORS CALIBRATION BY MEANS OF CONDITIONAL POLARIZATION ROTATION" G. Brida, M. Chekhova, M. Genovese, M.Gramegna, L. Krivitsky, M.L. Rastello, *Journ. Opt. Soc. of Am. B* **22** (2005) 488.
23. "TWIN-PHOTON TECHNIQUES FOR PHOTO-DETECTOR CALIBRATION", G. Brida, M.Genovese, M. Gramegna, *Laser Physics Lett.* **3** (2006) 115.
24. Giorgio Brida, Maria Chekhova, Marco Genovese, Alexander Penin, Ivano Ruo-Berchera, "The possibility of absolute calibration of analog detectors by using parametric down-conversion: a systematic study," *J. Opt. Soc. Am. B* **23**, 2185-2193 (2006).
25. I. Ruo Berchera, "Theory of PDC in a continuous variables framework and its applications to the absolute calibration of photo-detectors", *Adv. Sci. Lett.* **2**, 407429 (2009).
26. "Analysis of the possibility of analog detectors calibration by exploiting Stimulated Parametric Down Conversion", G.Brida, M. Chekhova, M.Genovese, I. Ruo-Berchera, *Optics Express*, Vol. 16 (2008) 12550.
27. G. Brida, M. Chekhova, M. Genovese, M.L. Rastello, I.Ruo Berchera, Absolute calibration of Analog Detector using Stimulated Parametric Down Conversion, *J. Mod. Opt.*, Vol. 56(2-3), 401-408 (2009).
28. T. Sh. Iskhakov, E. D. Lopaeva, A. N. Penin, G. O. Rytikov, and M. V. Chekhova, "Two Methods for Detecting Nonclassical Correlations in Parametric Scattering of Light", *JETP Letters*, 2008, Vol. 88, No. 10, pp. 660664.
29. Brida,G., Genovese,M., Meda, A., Predazzi, E. and Ruo Berchera, I., "Systematic study of the PDC speckle structure for quantum imaging applications", *Int. Journ. Quant. Inf.* **7** 139 (2009).
30. Brida,G., Genovese,M., Meda, A., Predazzi E. and Ruo Berchera, I., "Tailoring PDC speckle structure", *Journal of Modern Optics* **56** 201 (2009).
31. Ivan N. Agafonov, Maria V. Chekhova, Gerd Leuchs; "Two-Color Bright Squeezed Vacuum"; arXiv:0910.4831
32. "Guide to the expression of uncertainty in measurement (GUM)", ISO/IEC Guide 98:1995
33. "Radiometry, fotometry and the candela: evolution in the classical and quantum world", N.Fox,E.Ikonen,M.Rastello, G.Ulm, J.Zwinkels, in press.

## 1. Introduction

The possibility of realizing sub shot noise regime by exploiting multimode spatial correlation at the quantum level [1, 2], sometimes called spatial entanglement, has been experimentally demonstrated by using traveling wave parametric amplifier and CCD array detectors both at the single photon level [3] and at high photon flux [4, 5, 6, 7, 8], and by exploiting four wave mixing in rubidium vapors [10]. Very recently, following the proposal of [9] our group showed that it can find a natural application to the quantum imaging of weak absorbing object beyond the shot-noise-level [6](standard quantum limit). All these findings indicate that multimode spatial correlations and their detection is a mature field that can lead to other interesting applications. In particular, in this framework we developed the capability of an almost perfect spatial selection of modes that are pairwise correlated at the quantum level in parametric down conversion, and the optimization of the noise reduction below the shot-noise-level.

On the other side, quantum correlations of twin beams generated by Parametric Down Conversion (PDC), is a well recognized tool for calibrating single photon detectors, competing with the traditional ones of the optical metrology [11, 12, 13, 14, 15, 16, 17, 18, 20, 21, 22, 23]. Extending this technique to higher photon fluxes, for calibrating analog detectors, may have great importance in metrology [24, 26, 27, 25, 19, 28]. So far, the main problem to achieve this goal has been the difficulty of an accurate spatial selection of the correlated modes among the

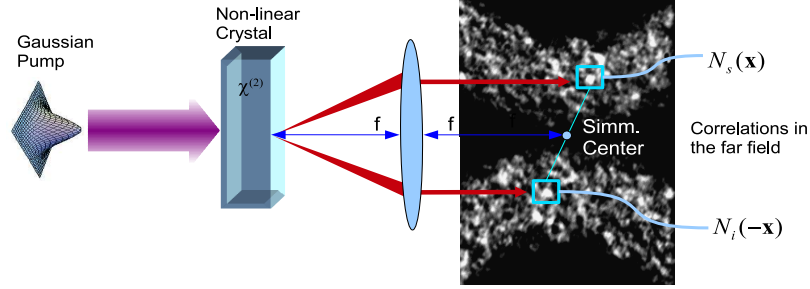


Fig. 1. Scheme for spatial correlations detection in PDC. The PDC emission from the non-linear crystal is detected in the far field, reached by a optical  $f - f$  configuration. The pump transverse size determines an uncertainty in the photon propagation direction. The speckled image showed, has been obtained experimentally in very high gain regime. For this reason, the spatial fluctuations are very strong, and the coherence area is roughly represented by the typical size of the speckles.

spatially broadband emission of PDC.

In the work presented here, the know-out in the detection of spatial correlation in PDC is fruitfully applied to the absolute calibration of CCD cameras. The method is based on the measurement of the degree of correlation between symmetric areas belonging to the twin beams, which in principle depends only by the transmission and detection efficiency. The achieved statistical uncertainty indicates the effectiveness of the methods for metrology applications.

## 2. Multimode spatial correlation in PDC

The state produced by spontaneous PDC, in the approximation of plane wave pump field of frequency  $\omega_p$  and propagating in the  $z$  direction, presents perfect transverse momentum phase-matching. Thus, it can be expressed as a tensor product of bipartite states univocally identified by frequency  $\omega_p/2 \pm \omega$  and transverse momentum  $\pm \mathbf{q}$ , i.e.  $|\Psi\rangle = \bigotimes_{\mathbf{q}, \omega} |\psi(\mathbf{q}, \omega)\rangle$ . Since we are mainly interested to the frequencies near to the degeneracy ( $\omega \sim 0$ ), the state of the single bipartite transverse mode reduces to

$$|\psi(\mathbf{q})\rangle = \sum_n C_{\mathbf{q}}(n) |n\rangle_{i, \mathbf{q}} |n\rangle_{s, -\mathbf{q}}, \quad (1)$$

where the coefficients  $C_{\mathbf{q}}(n) \propto \sqrt{\langle n_{\mathbf{q}} \rangle^n / \langle n_{\mathbf{q}} + 1 \rangle^{n+1}}$  are related to the mean number of photon in the mode  $\mathbf{q}$  assumed to be the same for all the modes, i.e.  $\langle n_{\mathbf{q}} \rangle = \mu$ , and the subscripts  $s$  and  $i$  indicated signal and idler fields.

The two-mode state in Eq. (1) is entangled in the number of photons for each pair of modes  $\pm \mathbf{q}$ , whereas the statistics of the single mode is thermal with mean value  $\langle n_{i, \mathbf{q}} \rangle = \langle n_{s, -\mathbf{q}} \rangle = \mu$  and variance  $\langle \delta^2 n_{i, \mathbf{q}} \rangle = \langle \delta^2 n_{s, -\mathbf{q}} \rangle = \mu(\mu + 1)$ . Now, we focus on the far field region, obtained as the focal plane of a thin lens of focal length  $f$  in a  $f - f$  configuration (Fig. 2). Here, any transverse mode  $\mathbf{q}$  is associated with a single position  $\mathbf{x}$  in the detection (focal) plane according

to the geometric transformation  $(2cf/\omega_p)\mathbf{q} \rightarrow \mathbf{x}$ , with  $c$  the speed of light. Therefore, a perfect correlation appears in the photon number  $n_{i,\mathbf{x}}$  and  $n_{s,-\mathbf{x}}$  registered by two detectors placed in two symmetrical positions  $\mathbf{x}$  and  $-\mathbf{x}$ , where the center of symmetry (CS) is basically the pump-detection plane interception (neglecting the walk off).

In real experiments the pump laser is not a plane wave, rather it can be reasonably represented by a gaussian distribution with spatial waist  $w_p$ . This induces an uncertainty in the relative propagation directions of the twin photons of the order of the angular bandwidth of the pump. This uncertainty is the coherence area of the process, roughly corresponding to the transverse size of the mode in the far field (see Fig. 2). The number of photons collected in symmetrical portions of the far-field zone are perfectly quantum correlated only when the detection areas  $\mathcal{A}_{det}$  are broader than a coherence area, whose size  $\mathcal{A}_{coh}$  is of the order of  $[(2\pi cf)/(\omega_p w_p)]^2$  [2, 9] (only for very large parametric gain it deviates from this behavior [9, 4, 29, 30]). Therefore, let us consider to collect photons over two perfectly symmetrical and correlated areas  $\mathcal{A}_{det,s}$  and  $\mathcal{A}_{det,i}$  with detection efficiency  $\eta_s$  and  $\eta_i$  belonging to the signal and idler beams respectively, and containing many transverse spatial modes  $\mathcal{M}_{spatial} = \mathcal{A}_{det,j}/\mathcal{A}_{coh}$  ( $j = s, i$ ). We also consider a situation in which the detection time  $\mathcal{T}_{det}$  is much larger than the coherence time  $\mathcal{T}_{coh}$  of the process, thus the number of temporal mode is large,  $\mathcal{M}_t = \mathcal{T}_{det}/\mathcal{T}_{coh} \gg 1$ . Since the modes in the single region are independent, the statistics is multithermal with mean value  $\langle N_j \rangle = \mathcal{M}_{tot} \eta_j \mu$  (with  $\mathcal{M}_{tot} = \mathcal{M}_t \mathcal{M}_{spatial}$ ) and variance

$$\langle \delta^2 N_j \rangle \equiv \langle N_j \rangle (1 + \mathcal{E}) = \langle N_j \rangle \left( 1 + \frac{\langle N_j \rangle}{\mathcal{M}_{tot}} \right) = \mathcal{M}_{tot} \eta_j \mu (1 + \eta_j \mu), \quad (2)$$

with  $j = s, i$  and  $\mathcal{E}$  the excess noise, usually defined as the fluctuations that exceed the shot noise level (SNL). The SNL, or standard quantum limit represents the level of noise associated to the detection of the coherent light, i.e.  $\langle \delta^2 N_j \rangle_{SNL} = \langle N_j \rangle$ . In this theoretical description, the excess noise is only related to the intrinsic thermal statistic of the single beam of PDC  $\mathcal{E} = \langle N_j \rangle / \mathcal{M}_{tot}$ . However, we will discuss in the following that experimental imperfections give the major contribution to the excess noise in our setup.

The covariance between the signal and idler numbers of photon is

$$\langle \delta N_i \delta N_s \rangle = \mathcal{M}_{tot} \eta_s \eta_i \mu (1 + \mu). \quad (3)$$

The amount of correlation between the signal and idler fields is usually expressed in terms of the noise reduction factor  $\sigma$  defined as the fluctuation of the difference  $N_- \equiv N_s - N_i$  between the photons number normalized to the corresponding level of shot noise:

$$\sigma \equiv \frac{\langle \delta^2 N_- \rangle}{\langle N_i + N_s \rangle} = 1 - \eta_+ + \frac{\eta_-^2}{2\eta_+} \left( \frac{1}{2} + \mu \right) = 1 - \eta_+ + \frac{\eta_-^2}{4\eta_+^2} \left( \eta_+ + \frac{\langle N_s + N_i \rangle}{\mathcal{M}_{tot}} \right), \quad (4)$$

where  $\eta_+ = (\eta_s + \eta_i)/2$  and  $\eta_- = \eta_s - \eta_i$ . It as been evaluated by introducing the Eq.s (3) and (2) in the expression of the fluctuation  $\langle \delta^2 N_- \rangle \equiv \langle \delta^2 N_s \rangle + \langle \delta^2 N_i \rangle - 2\langle \delta N_i \delta N_s \rangle$

In the case of perfect balanced losses  $\eta_s = \eta_i = \eta$  one get that  $\sigma = 1 - \eta$  only depending on the quantum efficiency. Therefore, in an ideal case in which  $\eta \rightarrow 1$ ,  $\sigma$  approaches zero. On the other side, for classical states of light the degree of correlation is bounded by  $\sigma \geq 1$ , where the lowest limit is reached for coherent beams,  $\sigma = 1$ .

According to Eq. (4), the absolute estimation of the quantum efficiency by measuring the noise reduction factor, can be achieved just when the excess noise disappears, that is realized in the case of balanced losses. The balancing of the two channels can be performed physically by adding proper absorbing filters in the optical paths. Anyway, a more convenient approach is to

compensate a posteriori, for instance multiplying the values of  $N_i$  for a factor  $\alpha = \langle N_s \rangle / \langle N_i \rangle = \eta_s / \eta_i$ . It corresponds to evaluate the redefined noise reduction factor  $\sigma_\alpha$  (instead of the one in Eq. (4)):

$$\sigma_\alpha \equiv \frac{\langle \delta^2(N_s - \alpha N_i) \rangle}{2 \langle N_s \rangle} = \frac{1}{2}(1 + \alpha) - \eta_s, \quad (5)$$

This relation shows that the quantum efficiency  $\eta_s$  can be evaluated measuring  $\sigma_\alpha$  and the ratio  $\alpha = \langle N_s \rangle / \langle N_i \rangle$ , without the need of a physical balancing the two optical paths.

As a final remark, we observe that the result in Eq. (5) relays on the assumption that each spatial modes collected by the region  $\mathcal{A}_{det,i}$  finds its correlated in the region  $\mathcal{A}_{det,s}$ , and viceversa. Otherwise, the presence of uncorrelated modes in the two region would not provide a complete cancelation of the excess noise by the subtraction, leading to underestimate the quantum efficiency [31]. Therefore, experimental control on the detection of the spatial modes by means of precise positioning and sizing of the regions and accurate determination of the CS is fundamental for the accuracy of the estimation of the quantum efficiency.

### 3. The experimental procedure

In our setup, a type II BBO non-linear crystal ( $l = 7$  mm) is pumped by the third harmonic (355 nm) of a Q-switched Nd:Yag laser. The pulses have a duration of  $\mathcal{T}_p = 5$  ns with a repetition rate of 10 Hz and a maximum energy, at the selected wavelength, of about 200 mJ. The pump beam crosses a spatial filter (a lens with a focal length of 50 cm and a diamond pin-hole, 250  $\mu\text{m}$  of diameter), in order to eliminate the non-gaussian components and then it is collimated by a system of lenses to a diameter of  $w_p = 1.25$  mm. After the crystal, the pump is stopped by a couple of UV mirrors, transparent to the visible ( $\simeq 98\%$  transmission at 710 nm), and by a low frequency-pass filter ( $\simeq 95\%$  transmission at 710 nm). The down converted beams (signal and idler) are separated in polarization by two polarizers (97% transmission) and finally the far field is imaged by a CCD camera. We used a 1340X400 CCD array, Princeton Pixis:400BR (pixel size of 20  $\mu\text{m}$ ), with high quantum efficiency (around 80%) and low noise in the read out process (4 electrons/pixel). The CCD exposure time is set by a mechanical shutter to 90 ms, thus each image acquired corresponds to the PDC emission generated by a single shot of the laser. The far field is observed at the focal plane of the lens with 10 cm focus in a  $f - f$  optical configuration.

For reasons related to the visibility of the correlation, and in order to reduce the contribution of the read noise of the CCD, it is convenient to perform an hardware binning of the physical pixels. It consists in grouping the physical pixels in squared blocks, each of them being processed by the CCD electronics as single "superpixel". Depending on the measurement, the size of the superpixel can be set accordingly. Typically we choose it of the same order, or larger than  $\mathcal{A}_{coh}$ .

The expected number of temporal modes  $\mathcal{M}_t = \mathcal{T}_p / \mathcal{T}_{coh}$  detected in one image is  $5 \cdot 10^3$ , considering the coherence time  $\mathcal{T}_{coh}$  of PDC around one picosecond. The number of spatial modes  $\mathcal{M}_{spatial} = \mathcal{A}_{det,j} / \mathcal{A}_{coh}$  ( $j = s, i$ ) depends only on the size of the detection areas, since  $\mathcal{A}_{coh} \sim 120 \times 120 (\mu\text{m})^2$  is fixed by the pump transverse size. The level of excess noise due to the thermal statistics in the single beam is also fixed, since we keep fixed (aside unwanted fluctuation pulse-to-pulse) the power of the laser. The total number of modes  $\mathcal{M}_{tot}$  turn out to be compatible with the level of excess noise  $\mathcal{E} \equiv \langle N_s \rangle / \mathcal{M}_{tot} \sim 0.1 - 0.2$ . It can be measured by performing spatial statistics as described in Sec. (3.1).

For an accurate estimation of quantum efficiency the following steps should be performed:

- a) *Determination of the center of symmetry (CS)*  
positioning of the correlated areas and determination of the center of symmetry of the

spatial correlations within sub-coherence-area uncertainty, according to the experimental procedure presented in Subsection (3.1)

b) *Determination of the minimum size of  $\mathcal{A}_{det,j}$*

The size of the detection areas must satisfy the condition  $\mathcal{M}_{spatial} = \mathcal{A}_{det,j} / \mathcal{A}_{coh} \gg 1$ , for the purposes of the unbiased estimation of  $\sigma$ . This can be achieved following the procedure sketched in Subsection (3.2).

c) *Analysis of experimental contributions to the excess noise*

Evaluation of noise coming from experimental imperfections, such as instability of the laser pulse-to-pulse energy and the background due to straylight and electronic noise of the CCD. Eq.s (6) and (7) are modified in order to account for these noise contributions. Detailed discussion on this item can be found in Subsection (3.3).

d) *Estimation of  $\eta_j$  and of its statistical uncertainty according to Eq. (5)*

$\alpha$  and  $\sigma_\alpha$  are estimated experimentally over a set of  $\mathcal{N}$  images according to formula

$$\alpha = \frac{E[N_s(k)]}{E[N_i(k)]}, \quad (6)$$

and formula

$$\sigma_\alpha = \frac{E[(N_s(k) - \alpha N_i(k))^2] - E[N_s(k) - \alpha N_i(k)]^2}{E[N_s(k)] + \alpha E[N_i(k)]}, \quad (7)$$

respectively, where  $E[N_j(k)] = \mathcal{N}^{-1} \sum_{k=1}^{\mathcal{N}} N_j(k)$ , and  $N_j(k)$  is the number of photons observed in the detection area  $\mathcal{A}_{det,j}$  in the  $k$ -th image. [See Subsection (3.4)].

e) *Evaluation of the optical losses*

The actual value for the estimated quantum efficiency  $\eta_j$  subsumes also losses due to the crystal, the lens and the mirrors. Thus, the value of the quantum efficiency of the CCD is obtained as the ratio between the estimated value for the quantum efficiency  $\eta_j$  and the transmission on the  $j$ -channel, i.e.

$$\eta_{true,j} = \frac{\eta_j}{\tau_j}, \quad (8)$$

with  $j = s, i$ .  $\tau_j$  should be evaluated by means of an independent "classical" transmittance measurement. As in this paper we present just a proof of principle of the proposed technique, we will not discuss this transmittance measurements anymore in this paper. Thus, instead of providing the quantum efficiency of the CCD standalone, the results presented in the following can be interpreted as the quantum efficiency of the whole optical system before the CCD, including the CCD itself.

### 3.1. determination of CS

The single shot image is stored as a "superpixel" matrix (Fig. 2). We select two equal rectangular regions  $\mathcal{A}_{det,s}$  and  $\mathcal{A}_{det,i}$  belonging to the signal and idler portion of the image and containing a certain number of "superpixels". In our case, we choose  $9 \text{ mm}^2$  areas that span a wavelength bandwidth of the order of 10nm around the degeneracy at 710nm. Fixing the region  $\mathcal{A}_{det,s}$ , we evaluate the noise reduction factor  $\sigma_{spatial}$  as a spatial average on the pairs of conjugated "superpixel" inside the two regions, in function of the position of the center of the region  $\mathcal{A}_{det,i}$  of coordinate  $\xi = (\xi_1, \xi_2)$ . In this way we obtain a matrix of values of the spatial average  $\sigma_{spatial}(\xi)$  as a function of the center  $\xi$  of the detection area  $\mathcal{A}_{det,i}$ .



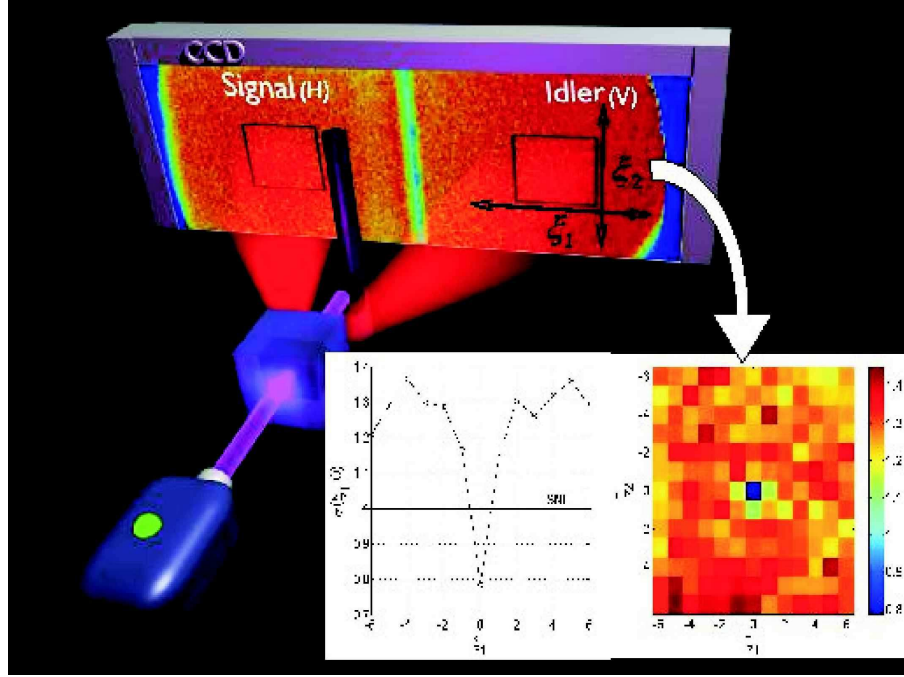


Fig. 2. Determination of center of symmetry. The right hand side presents a typical image obtained by the CCD in the working condition. The images is separated in two portions, one collecting the light from the signal beam (H-polarized) and the other the light of the idler beam (V-polarized). Two regions  $R_s$  and  $R_i$  (squares) are selected, and subtracted pixel by pixel. The spatial noise of the difference is reported in the inserts (right-bottom) in function of the position  $\xi = (\xi_1, \xi_2)$  of the idler region.

The result obtained by the analysis of a typical image are presented in Fig. 2, where a binning  $6 \times 6$  of the physical pixel has been applied and the number of photon per superpixel is  $\simeq 1700$ . The presence of correlations around  $\xi = 0$  is represented by a deep in the values of the spatial average of  $\sigma_{spatial}$ , whereas far from the minimum the correlation decrease, because conjugated pixels no more detect the correlated photons. Thus, this measurement of the spatial correlation allows to determine the best position of  $\mathcal{A}_{det,i}$  with respect to  $\mathcal{A}_{det,s}$ , and hence the center of symmetry of the correlation. The size of the correlation deep represents the coherence area that in our experiment is  $\mathcal{A}_{coh} \sim 120 \times 120 (\mu m)^2$ .

The superpixel size used for the measurement must realize a tradeoff between the visibility of the correlation, and the final uncertainty in the CS determination. On one side, as discussed in Sec.2, for a good visibility of the quantum correlation (and to increase the signal to electronic noise ratio) the "superpixel" area should be much greater than  $\mathcal{A}_{coh}$ . On the other side, a small pixel size will lead to a small uncertainty. We found that in our setup the best choice is a pixel size equal to the coherence area, that can be obtained by a  $6 \times 6$  binning, as in Fig. 2.

From the discussion above, it is clear that the measurement described allows a positioning of the two correlated (symmetrical) regions within a single "superpixel" uncertainty, while the center of symmetry is identify within half a "superpixel". However, it can be demonstrated that even a shift of a small fraction of "superpixel" with respect the real CS determine a increasing of the noise reduction factor [2, 9]. In practice, the optimization of the NRF by micro positioning

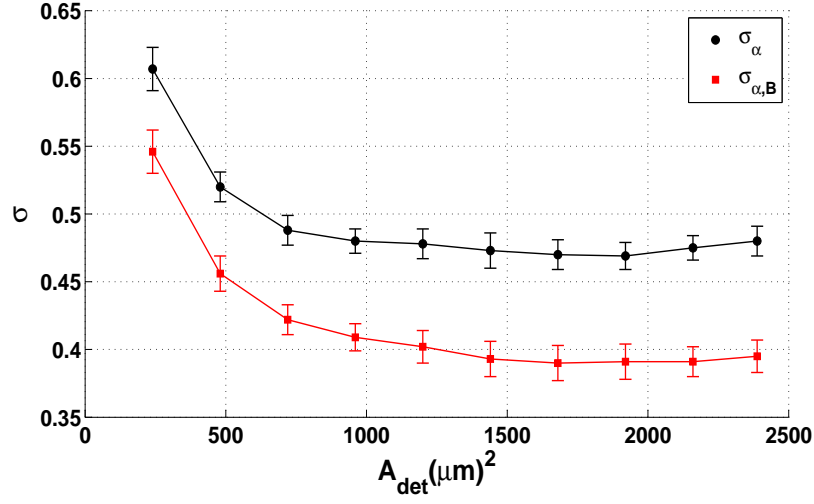


Fig. 3. Noise reduction factor in function of the detection area. x-axis reports the linear size of the detection areas in  $\mu m$ . The two experimental curves refer to the noise reduction factor  $\sigma_\alpha$  with (red), and without (black) background correction.

of the CCD allows to determine the physical center of symmetry within a final uncertainty less than 1/10 of the "superpixel", hence of the coherence area in our setup [2, 9].

### 3.2. Determination of the minimum size of $\mathcal{A}_{det,j}$

In the previous section we showed that CS can be determined with good precision, and the regions  $\mathcal{A}_{det,s}$  and  $\mathcal{A}_{det,i}$  are consequently fixed to be strictly symmetrical and correlated even "locally" (i.e. for each pair of twin spatial modes).

However, as pointed out in Sec. 2, perfect detection of quantum correlation requires the condition  $\mathcal{M}_{spatial} = \mathcal{A}_{det,j} / \mathcal{A}_{coh} \gg 1$ . In order to establish when this occurs, we measure the noise reduction factor in function of the detection area  $\sigma_\alpha(A_{det})$ , i.e. in function of the number of spatial modes detected. The measurement has been performed on a set of  $\mathcal{N} = 4000$  images using a binning  $12 \times 12$  that means a superpixel size of  $240 \times 240 (\mu m)^2$ . Here, we define  $N_j(k)$  the total number of photons detected in the region  $\mathcal{A}_{det,j}$  of the  $k$ -th image of the set.  $\sigma_\alpha(\mathcal{A}_{det,j})$  has been evaluated according to Eq. (7), over the set of 4000 images. Here, the single determination of the noise reduction factor is obtained by subtracting the total numbers of photons detected in the two large regions  $\mathcal{A}_{det,j}$  of the same image, and the statistics is obtained over the set of images. The results are reported in Fig. 3.

As expected,  $\sigma_\alpha(\mathcal{A}_{det,j})$  is a decreasing function reaching an asymptotic value for  $\mathcal{A}_{det,j} > \mathcal{A}_0 = 1440 \times 1440 (\mu m)^2$  that corresponds roughly to a number of spatial modes larger than 150. Therefore we can affirm that, working with detection area larger than  $\mathcal{A}_0$  allows to match the condition  $\mathcal{M}_{spatial} = \mathcal{A}_{det,j} / \mathcal{A}_{coh} \gg 1$ . This prevents possible bias in the estimation of quantum efficiency due to the uncertainty in the propagation direction of correlated photons.

### 3.3. Experimental contributions to the excess noise

Other sources of experimental noise lead to systematic issues on the experimental values of  $\sigma_\alpha$  and consequently on the quantum efficiency obtained by Eq. (5). In the following we will address this problems.



The largest contribution to the excess noise that we have in our setup is related to the instability of the Q-Switch laser pulse. In particular, we observed a fluctuation of the energy pulse-to-pulse of more than 10%. The power  $P$  of the pulse is directly related to the mean value of photons per mode  $\mu \propto \sinh^2(\text{const} * \sqrt{P})$ . Therefore, the temporal statistics of the PDC emission is drastically influenced by the pump power fluctuation. In particular  $\mu$  is not a constant. A temporal statistics on many pulses (many images) will be characterized by a mean value  $\bar{\mu}$  and variance  $V(\mu)$ . It can be demonstrated that the contribution of the pump fluctuation modifies the expected value of the noise reduction factor with respect to Eq.(4) in the form

$$\sigma \equiv \frac{\langle \delta^2 N_- \rangle}{\langle N_s + N_i \rangle} = 1 - \eta_+ + \frac{\eta_-^2}{2\eta_+} \left[ \bar{\mu} + \frac{1}{2} + \frac{V(\mu)}{\bar{\mu}} (1 + \mathcal{M}_{tot}) \right]. \quad (9)$$

From this equation it is clear that the instability of the pump generates a contribution to the amount of excess noise that can be relevant, since it includes a factor  $\mathcal{M}_{tot}$ .<sup>1</sup> Following the same argumentation of Section 2, the effect of this enhanced excess noise can be suppressed if the losses on the two beams are a posteriori compensated, by evaluating  $\sigma_\alpha$  instead of  $\sigma$ . In this case  $\sigma_\alpha$  reduces again to Eq. (5).

An other important source of excess noise is the background generated by the electronics of the CCD (digitalization, dark counts) and from the straylight, mostly caused by the fluorescence of the filter and mirrors used for stopping the pump, and residual of the pump itself. The first contribution, the electronic one, depends on the level of binning, and can be considered independent with respect to the thermal noise of the PDC, and straylight noise. In principle, also the straylight noise is uncorrelated with respect to the thermal fluctuation of the PDC light, and can be represented by a poissonian-like statistics. However, some correlation between the straylight and the PDC emission is introduced by the fluctuation of the pump, since when the pump pulse is more(less) energetic both the PDC and straylight increase (decrease) accordingly. Anyway it can be demonstrated that even this correlation cancels out in the difference of the photon number when the transmission of signal and idler path are balanced. We define the number of counts  $N'_{s/i}$  registered in the region  $R_{s/i}$  expressed as the sum of the PDC photons  $N_{s/i}$  and the background  $M_{s/i}$ .

The expression linking the quantum efficiency to the expectation value of measurable quantities in presence of background, the analogous of Eq. (5), is

$$\sigma_{\alpha,B} \equiv \frac{\langle \delta^2 (N'_s - \alpha_B N'_i) \rangle - \langle \delta^2 (M_s - \alpha_B M_i) \rangle}{2(\langle N'_s \rangle - \langle M_s \rangle)} = \frac{1}{2}(1 + \alpha_B) - \eta_s, \quad (10)$$

where  $\alpha_B \equiv \frac{\eta_s}{\eta_i} = \frac{\langle N'_s \rangle - \langle M_s \rangle}{\langle N'_i \rangle - \langle M_i \rangle}$ . The background and its statistics can be measured easily and independently, by collecting a set of  $\mathcal{M}$  images when the PDC is turned off, just by a 90° rotation of the crystal. Following the same formalism of point d) of the experimental procedure,  $\alpha_B$  is obtained as:

$$\alpha_B = \frac{E[N'_s(k)] - E[M_s(p)]}{E[N'_i(k)] - E[M_i(p)]}, \quad (11)$$

where  $E[N'_j(k)] = \mathcal{N}^{-1} \sum_{k=1}^{\mathcal{N}} N'_j(k)$ , and  $E[M_j(p)] = \mathcal{M}^{-1} \sum_{p=1}^{\mathcal{M}} M_j(p)$  represent the experimental determination of the quantum expectation values  $\langle N'_j \rangle$  and  $\langle M_j \rangle$  respectively. At the same time,  $\sigma_{\alpha,B}$  in Eq. (10) is obtained by the following experimental estimates:

$$\begin{aligned} \langle \delta^2 (N'_s - \alpha_B N'_i) \rangle &\mapsto E[(N'_s(k) - \alpha_B N'_i(k))^2] - E[N'_s(k) - \alpha_B N'_i(k)]^2 \\ \langle \delta^2 (M_s - \alpha_B M_i) \rangle &\mapsto E[(M_s(p) - \alpha_B M_i(p))^2] - E[M_s(p) - \alpha_B M_i(p)]^2 \end{aligned} \quad (12)$$

<sup>1</sup>The order of magnitude in our experiment is estimable as large as  $2\eta_+ \mathcal{M}_{tot} V(\mu) / \bar{\mu} = V(\langle N_s + N_i \rangle) / \langle N_s + N_i \rangle \sim 5 \cdot 10^3$  (see Tab. 1, first two columns). It is four orders of magnitude larger than the excess noise due to the thermal fluctuations.

We also mention that, for each measurement performed in the present work, the images affected by cosmic rays have been discarded by a proper algorithm.

### 3.4. Efficiency estimation and uncertainty evaluation

In the previous Subsections we have presented the procedure to obtain an unbiased estimation of the detection efficiency  $\eta_s$  by means of appropriate positioning and sizing the detection regions, a posteriori balancing of losses and background contribution analysis. In this subsection we present the experimental estimation of  $\eta_s$  as well as its uncertainty budget.

The sizing parameter chosen for this experimental proof of principle are: areas of detection  $\mathcal{A}_{det,j} = 2400 \times 3840 (\mu m)^2$  ( $5 \times 8$  superpixels of size  $480 \times 480 (\mu m)^2$  obtained by a binning  $24 \times 24$  of the physical pixels) corresponding to about  $640 \times \mathcal{A}_{coh}$ . The estimated value of  $\eta_s$  is obtained by the inversion of Eq. (10), where  $\alpha_B$  is calculated according to Eq. (11) and  $\sigma_{\alpha,B}$  performing the substitutions in Eq.s (12) on the basis of  $\mathcal{N}$  images with PDC light, and  $\mathcal{M}$  of background light.  $\eta_i$  can be obviously evaluated as  $\eta_i = \alpha_B \eta_s$ .

Once we intend to provide an uncertainty associated to the estimated value of  $\eta_s$  (and  $\eta_i$ ), we should repeat the experiment  $\mathcal{Z}$ -times, i.e. we should collect  $\mathcal{Z} \cdot \mathcal{N}$  images with PDC light, and  $\mathcal{Z} \cdot \mathcal{M}$  with background light. Thus the estimated value of  $\alpha_B$  and  $\sigma_{\alpha,B}$  can be obtained from

$$\alpha|_{estim} = \mathcal{Z}^{-1} \sum_{l=1}^{\mathcal{Z}} \alpha(l) \quad \sigma_{\alpha}|_{estim} = \mathcal{Z}^{-1} \sum_{l=1}^{\mathcal{Z}} \sigma_{\alpha}(l) \quad (13)$$

and the associated uncertainty is obtained following the guidelines of Ref. [32]. Specifically the uncertainty propagation is performed on the  $2\mathcal{N} + 2\mathcal{M}$  measured quantities, namely  $N'_s(k)$ ,  $N'_i(k')$ ,  $M_s(p)$ ,  $M_i(p')$  with  $k, k' = 1, \dots, \mathcal{N}$  and  $p, p' = 1, \dots, \mathcal{M}$ . We accounted for the correlations between  $N'_s(k)$  and  $N'_i(k')$  when  $k = k'$ , due mainly to PDC light, and between  $M_s(p)$  and  $M_i(p')$  when  $p = p'$ , due to pulse-to-pulse laser energy instability. Thus, it is assumed that there is no correlation between measured quantities in different images. In our experiment  $\mathcal{N} = \mathcal{M}$  and  $\mathcal{N} = 500$  and  $\mathcal{Z} = 8$ .

The estimated values of  $\alpha_B$  and  $\sigma_{\alpha,B}$  together with their uncertainties are presented in Table 1, where, for the sake of comparison, are shown also the corresponding values without background subtraction ( $\alpha$  and  $\sigma_{\alpha}$  respectively). According to Eq. (10) we obtained  $\eta_s = 0.613 \pm 0.011$ .

We underline that the estimated value of  $\eta_s$  corresponds to the efficiency of the whole quantum channel including the CCD -not only the efficiency of the CCD itself-, and that the uncertainty associated to  $\eta_s$  accounts only for the statistical contributions due to the fluctuations of the  $N$ -s and  $M$ -s measured quantities (Type A uncertainty contributions, according to Ref. [32]).

Typically, further non-statistical uncertainties contributions (Type B [32]) should be accounted for in a complete uncertainty budget. For example, in this case a proper evaluation of  $\alpha_B$  with small uncertainty is mandatory to nullify the effect of the excess noise in Eq. (9), i.e. to ensure the validity of Eq. (10). A Type B uncertainty contribution associated to the nullification of excess noise term should be considered. In Section 3.3 we showed that the excess noise due to the pulse to pulse instability is of the order of  $5 \cdot 10^3$  (see Footnote). From Eq. (9) it turns out that the condition for neglecting that term is  $\eta_-^2 / (4\eta_+^2) \cdot 5 \cdot 10^3 \ll 1$ , that in our case means  $\eta_- \ll 10^{-2}$ . The uncertainty on  $\alpha_B$  presented in table 1, shows that the balancing of the two arms can be performed within  $10^{-5}$ , equivalent to the condition  $\eta_- = 10^{-5}$ . Thus, the possible contribution to the uncertainty due to this term is less than  $10^{-6}$ .

In the determination of  $\sigma_{\alpha,B}$  this uncertainty contribution is several order of magnitude below the statistical (Type A) contributions, thus, absolutely negligible in the complete uncertainty budget. A larger Type B contribution comes from the bias in the determination of the center of symmetry that in our present experiment is 1/10 of the coherence area in both the coordinates

$E[N'_s]$	$\sqrt{E[\delta^2 N'_s]}$	$E[M_s]$	$\sqrt{E[\delta^2 M_s]}$	$\alpha^{estim}$	$\alpha_B^{estim}$	$\sigma^{estim}$	$\sigma_\alpha^{estim}$	$\sigma_{\alpha,B}^{estim}$
262710 (620)	35982 (437)	12751 (158)	1318 (30)	0.99952 (0.00003)	0.99416 (0.00004)	0.454 (0.010)	0.449 (0.010)	0.384 (0.011)

Table 1. Experimental estimates (row 2) and their uncertainties (row 3). Column 1-2 show the mean counts in the detection area  $\mathcal{A}_{det,s}$  of the single images and the mean square of fluctuation  $\delta^2 N'_s(k) = (N'_s(k) - E[N'_s])^2$ . Column 3-4 report the same values related to the background images. Column 5-6 present the experimental values of the compensation factor  $\alpha$  and the value corrected for background counts. In column 7-9 are reported the raw noise reduction factor, the one after compensation of the losses, and finally the one after compensation and background correction respectively.

in the detection plane. Following the argumentation at the end of section 3.1 it generates an uncertainty of 1.5%. The actual relative uncertainty in the estimation of  $\eta_s$  is 2.3%, it is expected that it can be easily reduced of more than one order of magnitude increasing the number of collected images, as far as the bottleneck of Type B uncertainty contribution is reached.

#### 4. Discussions and Conclusions

As a test of consistency for the theoretical model at the basis of the proposed CCD calibration technique, and, in particular, for the associated uncertainty model we evaluate the statistical uncertainty associated to the mean values of  $\alpha_B$  and  $\sigma_{\alpha,B}$ , according to

$$\Delta\alpha^{estim} = \sqrt{[\mathcal{Z}(\mathcal{Z}-1)]^{-1} \sum_{l=1}^{\mathcal{Z}} [\alpha(l) - \alpha^{estim}]^2} \quad (14)$$

$$\Delta\sigma_\alpha^{estim} = \sqrt{[\mathcal{Z}(\mathcal{Z}-1)]^{-1} \sum_{l=1}^{\mathcal{Z}} [\sigma_\alpha(l) - \sigma_\alpha^{estim}]^2},$$

obtaining a good agreement with the estimated uncertainty.

Furthermore, we observe that according to the principle that the accuracy of a measurement depends on the measuring time (in our case the number of acquired images), and not depend on how the data are arranged, we verified that the final uncertainty on the mean values is not influenced by the different possible choices of  $\mathcal{Z}$  and  $\mathcal{N}$ , provided that total number of images  $\mathcal{Z} \cdot \mathcal{N} = \text{const}$ . On the contrary, the standard deviation of the populations, is a function of  $\mathcal{N}$ , as it is shown in Fig. 4.

We note that Tab.1 shows that  $\langle M_s \rangle$  is 5% of the total counts  $\langle N'_s \rangle$  although the weigh of background correction is the 15% of the estimated noise reduction factor. Nevertheless, the uncertainty on the value of  $\sigma_{\alpha,B}$  is just slightly influenced by the background correction. For the sake of completeness we observe that the electronic noise contributes with a standard deviation  $\Delta \sim 70$  counts. In a forward-looking perspective, for pushing the uncertainty on this measurements at the level of the best values obtained in the single photon counting regime, it would be very important to reduce the straylight. Actually it is possible to design a different experimental configuration that limits the fluorescence of the pump.

In conclusion we have proposed and demonstrated experimentally a new method for the absolute calibration of analog detector based on measuring the sub-shot-noise intensity correlation between two branches of parametric down conversion. The results on the calibration of a scientific CCD camera demonstrate the metrological interest of the method, that could find various applications, starting from the possibility to give a key element for redefining candela

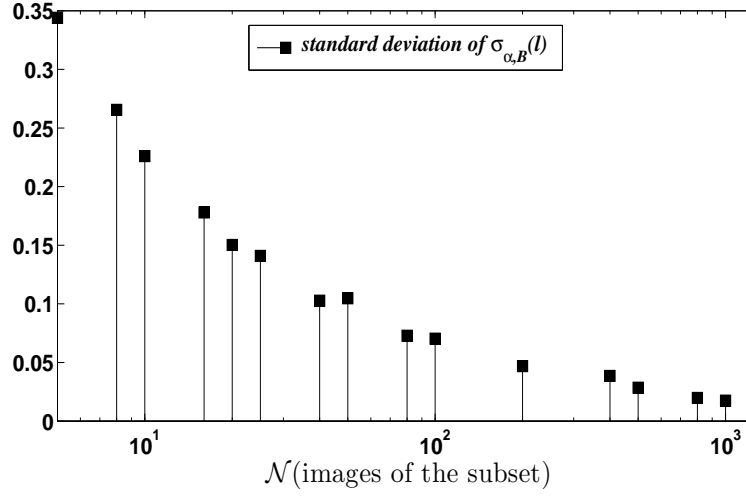


Fig. 4. Standard deviation of  $\sigma_{\alpha,B}$  on a number  $\mathcal{L}$  of independent measurements. In each measurement a value of  $\sigma_{\alpha,B}$  is obtained by formula (10) with the substitutions (12), using a set of  $\mathcal{N}$  images. Although the standard deviation of the population decrease for larger  $\mathcal{N}$ , the uncertainty on the mean value, only depends on the total number of images  $\mathcal{L} \cdot \mathcal{N}$  [See text for further discussion].

unit [33] in terms of photo-counting.

#### Acknowledgments

This work has been supported in part by MIUR (PRIN 2007FYETBY), NATO (CBP.NR.NRCL.983251) and QuCandela EU project.